Journal of Electronic Materials (2023) 52:3394–3400
https://doi.org/10.1007/s11664-023-10319-8

ORIGINAL RESEARCH ARTICLE

Effect of the Second-Phase Particle Distribution on the Brittle Fracture Behavior of Sn-3Ag-0.5Cu Solder

Xiangxi Zhao[1] · Wei Zhang[1] · Chunqing Wang[1] · Wei Liu[1] · Chunjin Hang[1]

Received: 9 October 2022 / Accepted: 17 February 2023 / Published online: 7 March 2023

Abstract

The low-temperature impact test was used to examine the fracture morphology of Sn-3Ag-0.5Cu (SAC305) solder. The second-phase distribution of Ag_3Sn and Cu_6Sn_5 particles on the grain boundary of SAC305 solder was obtained using a nanometer-scale focused ion beam and observed using a transmission electron microscope. The results show that as the temperature drops, the fracture mode of SAC305 solder shifts from ductile to brittle, and that the fracture mode is primarily influenced by crystal morphology. On the grain boundaries of the crystal, a large number of Ag_3Sn particles and fewer Cu_6Sn_5 particles are discovered. The compositional analysis of the nanometer-scale fracture morphology reveals that the majority of the Cu elements are dispersed in the Sn matrix. The phase diagram and Sn activity help to understand this occurrence. The inhibitory effect of Ag on the creation of Cu compounds is further discussed, which not only promotes the connection between the soldering material and the Cu solder disc, but also reduces the fracture problem produced by the Cu_6Sn_5 second-phase particles.

Keywords SAC305 solder · ductile–brittle fracture · second-phase particles · intermetallic compounds

Introduction

As the dangers of lead become more widely recognized, more lead-free solders are being used in the manufacture of electronic devices. Sn-Ag-Cu solders are frequently regarded as the most plausible alternatives to Sn-Pb solders, due to their superior mechanical characteristics and solderability.[1,2] Researchers have discovered that proper intermetallic compounds (IMC) can help form a good metallurgical bonding interface, but as IMC grows during subsequent service, its composition, morphology, and thickness may change, affecting solder performance and the interfacial connection properties of the solder joint.[3–6] Different types of lead-free soldering materials will form different IMCs. The two most prevalent IMCs at the moment are Cu_6Sn_5 and Ag_3Sn, both of which form at grain boundaries when they are present alone. However, depending on where they are located inside a material, their existence will affect the material differently. Because the generation of IMCs is unavoidable during the soldering process, many methods for improving the performance and reliability of soldering materials have been investigated. With control of IMC morphology being considered a feasible method, many studies on IMCs have been conducted, focusing on grain morphology, external conditions, and filler metal composition.[7–11] Most grain morphology studies have shown that IMCs with smaller thicknesses form stable connections, whereas thicker IMCs cause stress concentration at the interface during thermal cycling, resulting in brittle fracture. The soldering interface is more likely to fail in service if the IMC is thicker.

When two IMCs, Ag_3Sn and Cu_6Sn_5, were present simultaneously, various studies found that a small amount of Ag was able to inhibit the generation of Cu_6Sn_5, resulting in higher reliability of the solder. Lee et al.[12] investigated the wettability and interfacial response of Sn-xAg-0.5Cu alloy, where the Ag content was at $x = 1$. The results showed that the filler metal with low Ag content inhibited the formation of Cu_6Sn_5 and Cu_3Sn, due to the small diffusion coefficient of Ag_3Sn growth, which improves reliability against drop shocks. Zhu et al.[13] conducted a comparative study on the microstructure and mechanical strength of alloyed and doped

✉ Wei Zhang
zhangw@hit.edu.cn

✉ Chunqing Wang
wangcq@hit.edu.cn

1 State Key Laboratory of Advanced Welding and Joining, Harbin Institute of Technology, Harbin 150001, China

Ag-modified Sn-0.7Cu solders, which were classified as Sn-0.7Cu solder, Sn-0.7Cu-0.3Ag and Sn-0.7Cu + 0.3Ag. The experimental results showed that the mechanical strength and electromagnetic resistance of Sn-0.7Cu solder could be improved by adding Ag to the solder. The excellent performance of Sn-0.7Cu-0.3Ag was due to the smaller size and wider distribution of Ag_3Sn in the solder matrix.

The methods described above are not the only ways to improve IMC properties. The majority of previous literature has focused on improving solder properties rather than explaining the reasons for the IMC inhibitory effect in detail. Unlike the previous studies, we obtain nanometer-scale grain boundary images from brittle fracture morphology, analyze Ag and Cu formation by morphology, location, and quantity, and explain the inhibitory effect of Ag on Cu_6Sn_5 generation in this paper.

Experimental Procedure

SAC305 eutectic alloy was made from 99.999% pure Sn, Ag, and Cu ingots in an induction furnace at over 1000°C for 40 min, and the SAC305 solder bar was cast into rectangular specimens measuring 55 mm × 10 mm × 10 mm with a 45° V-notch. The size marking of the impact standard specimen is shown in Fig. 1. The samples were placed in an incubator, which was cooled by liquid nitrogen, and the temperature of the incubator was controlled by a computer. Each sample was stored in the incubator for 10 min before impact test. Each data point represented the average impact energy of three specimens, and the impact curves were generated via Charpy impact testing at temperatures ranging from −150 to 20°C. A Zeiss scanning electron microscope (SEM) was used to view the low-temperature cracks and collect microscopic morphologies down to the micron scale. Focused ion beam (FIB) technology was utilized to cut the solder during the trials in order to more closely analyze the second-phase particle distribution. Under the electron microscope, it was discovered that the grain boundaries of the second-phase particles Ag_3Sn and Cu_6Sn_5 coexisted. A protective layer was applied to the second-phase particles to prevent fracture during cutting. Then, the vertical grain boundaries were cut using the FIB toward the interior of the solder. Finally, a tiny piece of the sample was produced for transmission electron microscopy (TEM) observation. Under the TEM, not only is the morphology of the grain boundary region obtained at the nanoscale, but the sample composition can also be examined and the location of the second-phase particles can be seen.

Results and Discussion

The Low-Temperature Impact Curve of SAC305 Solder

The low-temperature impact curve of SAC305 solder is shown in Fig. 2. The upper platform region of the impact curve is −40°C to 20°C, and the fracture mode is ductile fracture. The lower platform region of the impact curve is −150°C to −50°C, and the fracture mode is brittle fracture. The ductile–brittle transformation temperature range is between −50°C and −40°C, as stated by the definition of the term. The shift of the SAC305 solder from ductile to brittle can be generally reflected by the impact curve, but a more in-depth analysis that takes into account the dispersion of the second-phase particles must be stated using fracture morphology analysis.

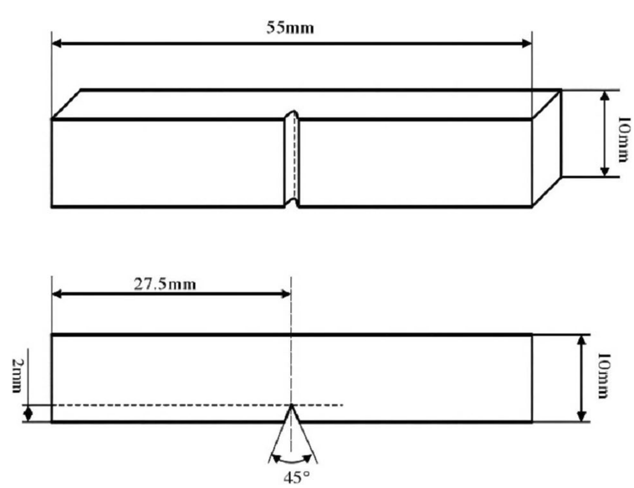

Fig. 1 The size marking of the impact standard specimen.

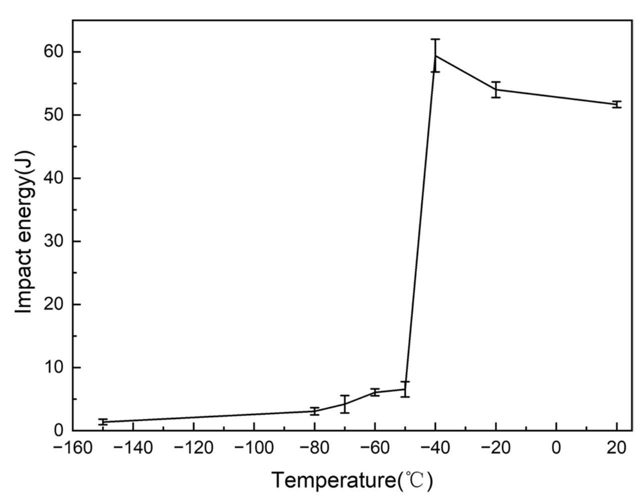

Fig. 2 The low-temperature impact curve of SAC305 solder.

Low-Temperature Fracture Morphology of SAC305 Solder

The difference of the low-temperature impact power of solder can be reflected in its fracture morphology. Because our research point is the process of ductile–brittle transformation, we divide the microscopic image into two parts for observation. The low-temperature fracture morphology of SAC305 from 20 to −40°C is shown in Fig. 3, and the low-temperature fracture morphology of SAC305 from −50°C to −150°C is shown in Fig. 4.

Obvious plastic deformation is observed in Fig. 3. The dimples became smaller with decreasing temperature, indicating a gradual decrease in ductility, and tearing edges due to plastic deformation are found in Fig. 3c. Dimples and tearing edges indicated that the solder was ductile fracture at this time. The microstructure of the fracture near the V-notch at −50°C is shown in Fig. 4a. The presence of several tough nests close to the V-notch is a clear indicator of ductile fracture. Typically, the bottom of the hard nests contains second-phase particles. Due to the specimen's tensile or shear deformation, the interface between the second-phase particles and the matrix initially cracked to form a crack source. As the stress increased, the amount of deformation increased, the dimples gradually tore open, and the tough nest formed protruding tearing edges due to plastic deformation, which was visible in the secondary electron image. The fracture morphology showed cleavage fractures, which indicated brittle fracture at low temperatures. The brittle fracture continued toward the center of Fig. 4b fracture morphology, commencing at the V-notch, where plastic deformation (slip band and dimples) occurred initially, indicating that the ductile–brittle transition had already taken place. Figure 4c shows a river pattern, which is a typical characteristic of brittle fracture mode. Starting with the V-notch in Fig. 4d, there is no plastic deformation. The separation phenomenon of the second-phase particles from the matrix is found immediately next to the V-notch. The transgranular and intergranular fractures seen in the image are typical features of brittle fractures. The fracture in Fig. 4e is completely brittle, with many second-phase particles pulling out on the fracture. Because the strength of the second-phase particles is greater than that of the matrix, the matrix cracked first when bearing, but the second-phase particles did not fracture. The matrix and the second-phase particles interface debond as the load increases, until the load reaches the second-phase particle

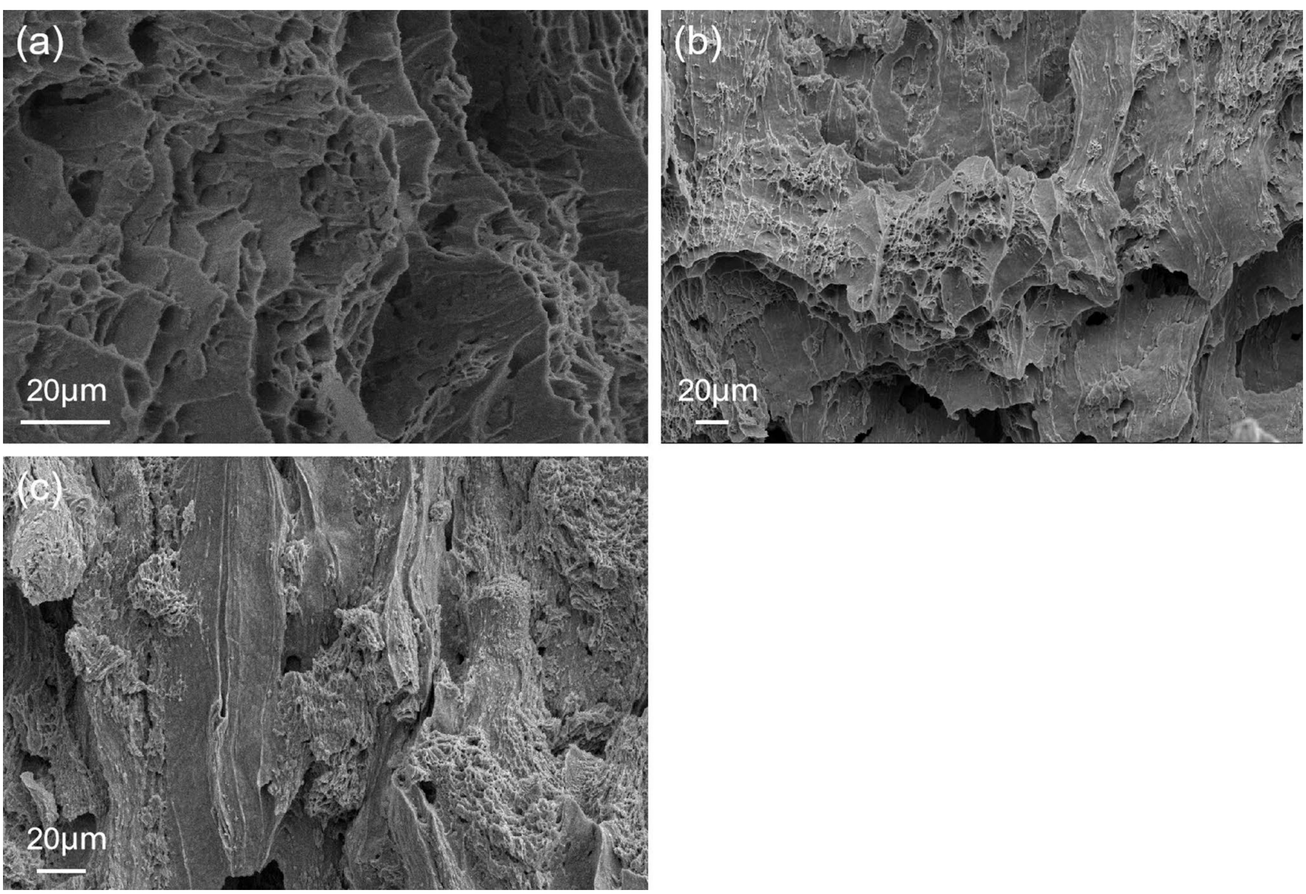

Fig. 3 Low-temperature fracture morphology of SAC305 from 20°C to −40°C: (a) 20°C; (b) −20°C; (c) −40°C.

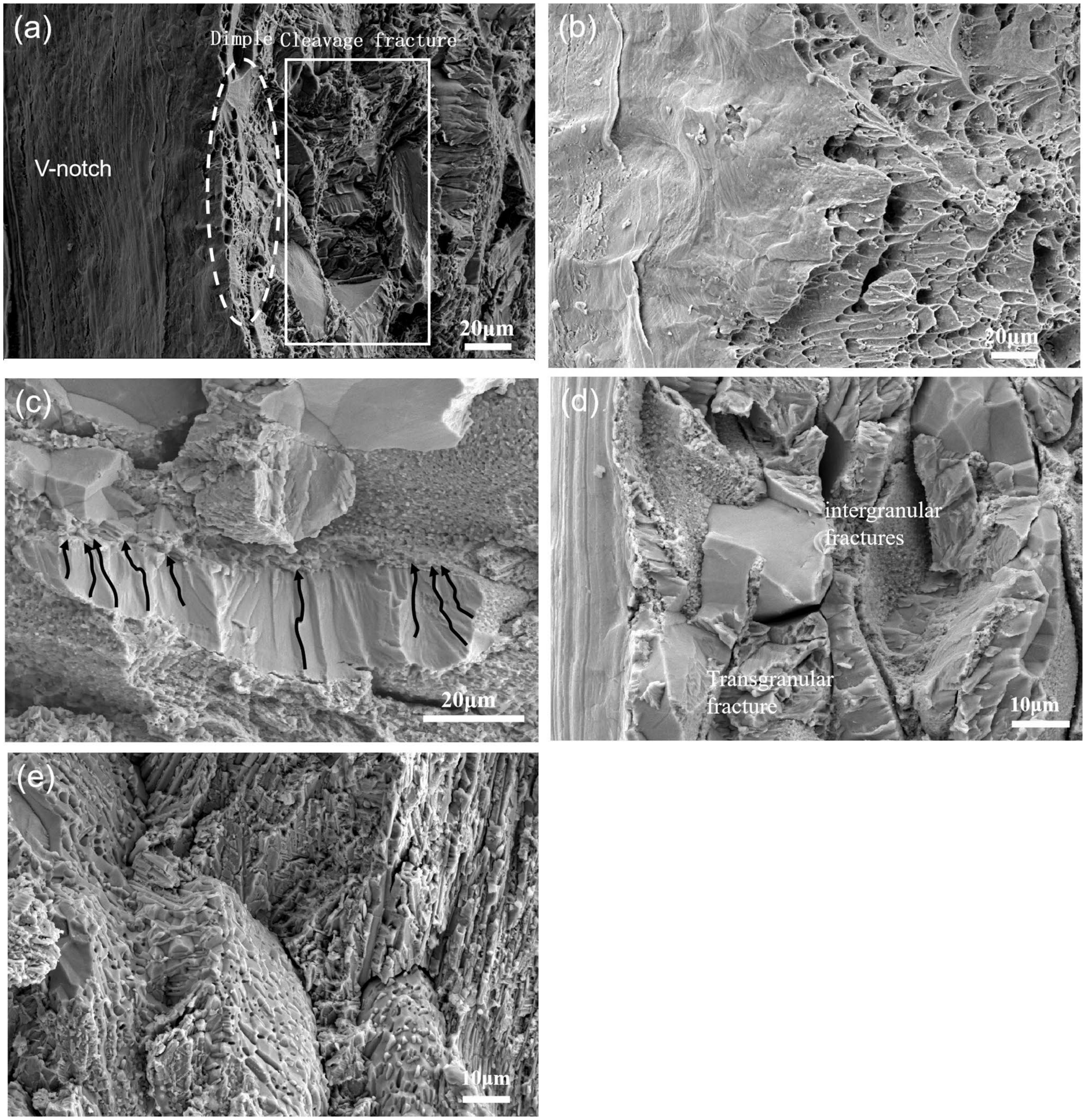

Fig. 4 Low-temperature fracture morphology of SAC305 from −50°C to −150°C: (a) −50°C; (b) −60°C; (c) −70°C; (d) −80°C; (e) −150°C.

fracture strength, at which point the second-phase particles fracture.

The fracture morphology and energy spectrum of Ag_3Sn and Cu_6Sn_5 at −80°C is shown in Fig. 5. The energy spectrum at region A is shown in Fig. 5b, and the energy spectrum analysis reveals Cu_6Sn_5. The energy spectrum at region B is shown in Fig. 5d, and the energy spectrum analysis reveals Ag_3Sn. The fracture morphology along the crystal contains a large number of Ag_3Sn particles of various shapes and sizes, while only a few Cu_6Sn_5 particles are present in large pieces at the interface. Because the reason for the large distribution of Ag_3Sn and the small amount of Cu_6Sn_5 could not be observed in the micrometer morphology, the fracture of SAC305 was observed in this paper by TEM at a smaller nanometer level.

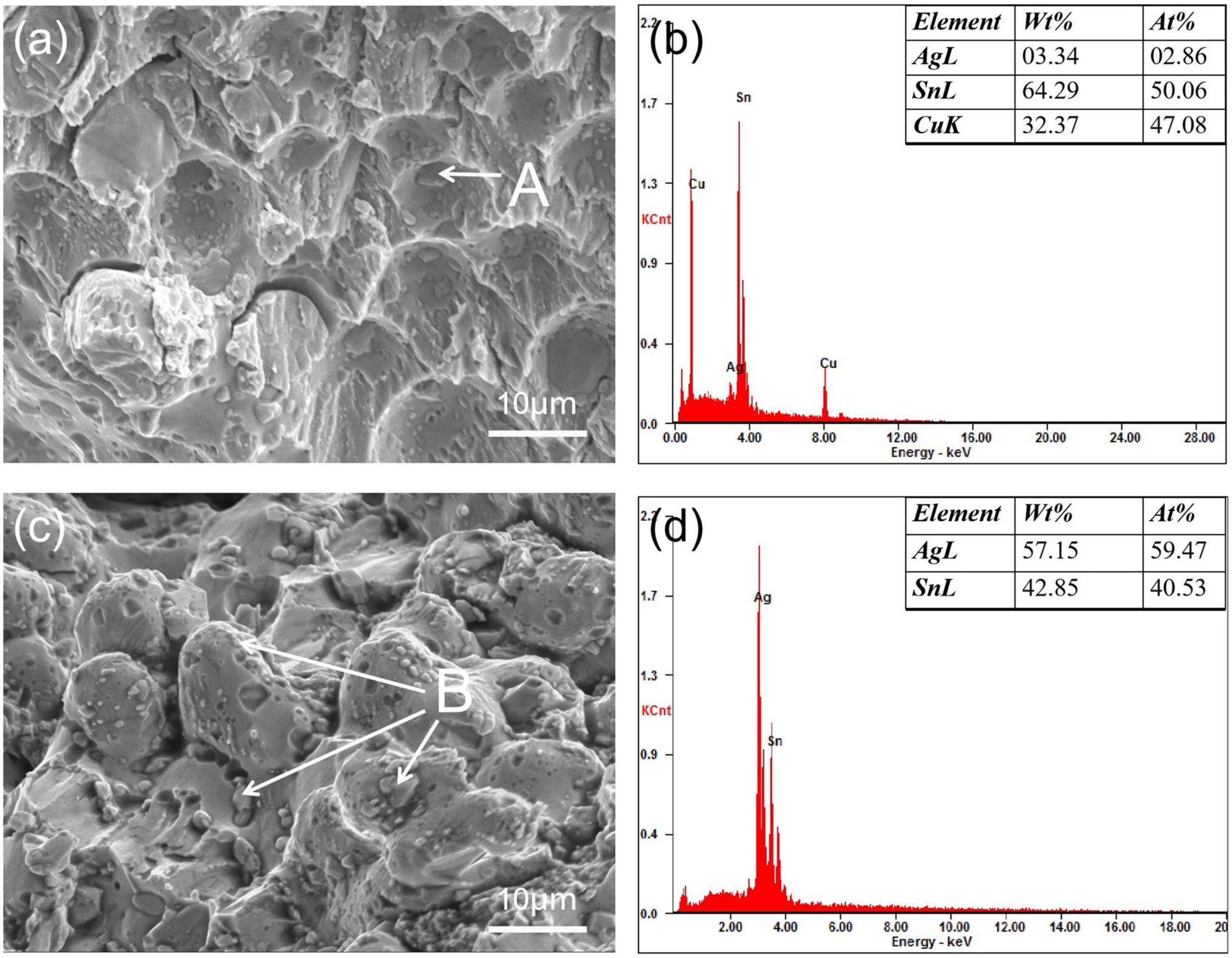

Fig. 5 Fracture morphology and energy spectrum of Ag_3Sn and Cu_6Sn_5 at −80°C: (a, c) SAC305 fracture morphology; (b) Cu_6Sn_5 energy spectrum; (d) Ag_3Sn energy spectrum.

The Second-Phase Particle Distribution of SAC305 Solder

Two adjacent second-phase particles were selected for FIB cutting at the SAC305 fracture to obtain a more visual distribution of the second-phase particles; the images and compositional analysis of the SAC305 specimen under TEM are shown in Fig. 6. The large Cu_6Sn_5 particle is elongated, whereas the Ag_3Sn particle is positioned in three different ways. First, the fracture interface has the largest prismatic particle, with the Cu_6Sn_5 particle on the left and the Sn matrix on the right. Second, the medium-sized oval Ag_3Sn particles are surrounded by Cu_6Sn_5 particles on half of their length, with the Sn matrix on the left. Finally, three Cu_6Sn_5 particles and the largest Cu_6Sn_5 particle completely surround the round Ag_3Sn particles. Second-phase particles tend to aggregate at grain boundaries in general; both Ag_3Sn particles and Cu_6Sn_5 particles are produced at grain boundaries, albeit in different environments. Ag elements are more concentrated than Cu elements, and can be further used to investigate the distribution pattern of the second-phase particles.

Distribution Mechanism of Second-Phase Particles in Sn-based Solder

The formation of the second-phase particles is related not only to the external temperature, but also to the solid solution degree of the element in the solder matrix. The solid solubility of an element can be represented by the binary phase diagram of the element and Sn. According to the “like dissolves like” theory, the melting points of Ag and Sn are so different that the solubility of a small amount of Ag in the eutectic composition is negligible, and almost all of the Ag forms Ag_3Sn particles. The microstructure of Sn-3.5Ag solder consists of ε-Ag_3Sn and β-Sn eutectic structures. The strength and hardness of the Ag_3Sn second-phase particles

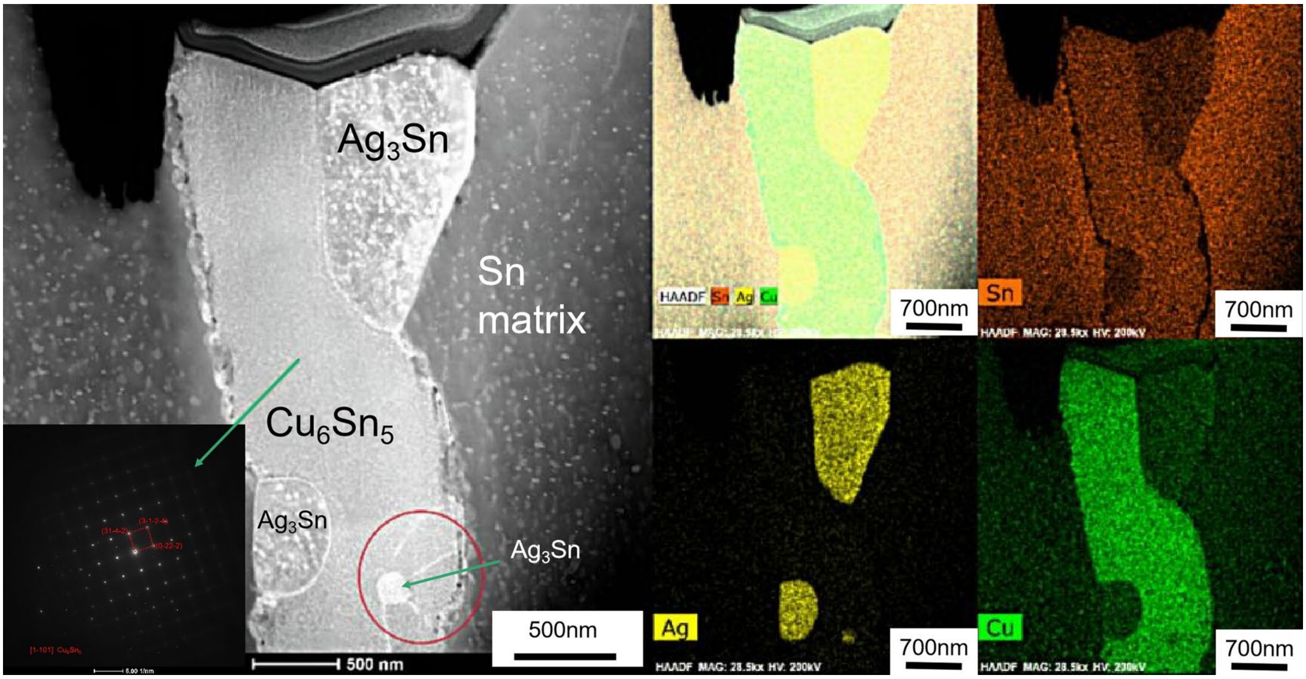

Fig. 6 The images and compositional analysis of the SAC305 specimen under transmission electron microscopy.

are higher than those of the Sn matrix, which can hinder dislocations and strengthen the alloy. Therefore, Ag_3Sn particles are more likely to aggregate at grain boundaries. Also, the presence of Ag_3Sn inhibits the mobility and diffusion of Sn, limiting the generation of boundary behavior.

By comparing the solubility curves of Sn in Ag and Cu, it can be found that Sn has greater solubility in Ag at the same temperature. According to diffusion kinetics, the driving force of IMC formation depends on the activity of its components.[14] For Cu_6Sn_5, its driving force ΔG depends on the activity at the Sn interface, which satisfies the formula:

$$\Delta G = -RT \ln \mu_{Sn} \tag{1}$$

where ΔG is the driving force for the formation of IMC; *R* is a constant; *T* is welding temperature; *μ* is the activity coefficient of Sn at the interface.

It can be seen from the formula that decreasing the activity of Sn atoms can effectively inhibit the growth of Cu_6Sn_5 at the interface, and related studies have found that ΔG can be changed by adding alloying elements such as Ag, Ni, Sb, and Au. The addition of Ag reduces the driving force for the formation of Cu_6Sn_5, thus inhibiting the formation of Cu_6Sn_5 and making its grains finer. The effect of Ag atoms on the Gibbs energy ΔG of the Cu-Sn system was similarly pointed out by Ma et al.[15] Since Ag cannot be dissolved in Cu_6Sn_5 and Cu_3Sn, the only way it can affect the interfacial reaction is to affect the activity of the reaction elements.[16] In addition, according to the adsorption theory of surfactant materials, the precipitated-phase Ag_3Sn adsorbed around Cu_6Sn_5 helps to reduce the surface energy of Cu_6Sn_5 grains and inhibit its growth.[17] As shown in Fig. 6, a small amount of Cu compounds gathered at the interface, but a large amount of Cu compounds were dispersed in the matrix. In conclusion, in lead-free soldering with Cu, we can take advantage of the inhibitory effect of the presence of Ag in the soldering material on Cu compounds to hinder the generation of Cu_6Sn_5 or Cu_3Sn at the interface and reduce the incidence of interfacial fracture aging behavior caused by IMC.

Conclusions

This study examined the ductile–brittle transition process of SAC305 solder from −150°C to 20°C, with a focus on low-temperature mechanical properties. We discovered that different fracture modes have different morphologies, and Ag_3Sn and Cu_6Sn_5 particles were more likely to be produced at grain boundaries, using low-temperature fracture morphologies. We used FIB and TEM to obtain nanometer-scale morphology of the distribution of second-phase particles inside the solder. We discovered that Ag_3Sn particles were more likely to aggregate at grain boundaries, and more Cu elements were dispersed in the matrix. Diffusion kinetics can identify this phenomenon; the driving force for IMC formation is determined by the activity of its constituents.

Acknowledgments This work was supported by the National Natural Science Foundation of China (No. U1537207)

Conflict of interest The authors declare that they have no known competing financial interests or personal relationships that could have appeared to influence the work reported in this paper.

References

1. C. Wu, D.Q. Yu, C. Law, and L. Wang, Properties of lead-free solder alloys with rare earth element additions. *Mater. Sci. Eng. R: Rep.* 44, 1–44 (2004).
2. J.W. Yoon, S.W. Kim, and S.B. Jung, Interfacial reaction and mechanical properties of eutectic Sn-0.7Cu/Ni BGA solder joints during isothermal long-term aging. *J. Alloy Compd.* 391, 82–89 (2005).
3. L. Qu, N. Zhao, H.J. Zhao, M.L. Huang, and H.T. Ma, In situ study of the real-time growth behavior of Cu_6Sn_5 at the Sn/Cu interface during the soldering reaction. *Scripta Mater.* 72–73, 43–46 (2014).
4. J.W. Yoon, H.S. Chun, and J.M. Koo, Microstructural evolution of Sn-rich Au-Sn/Ni flip-chip solder joints under high temperature storage testing conditions. *Scripta Mater.* 56, 661–664 (2007).
5. A. Sharif, M.N. Islam, and Y.C. Chan, Interfacial reactions of BGA Sn-3.5%Ag-0.5%Cu and Sn-3.5Ag solders during high-temperature aging with Ni/Au metallization. *Mater. Sci. Eng. B.* 113, 184–189 (2004).
6. S.F. Choudhury and L. Ladani, Local shear stress-strain response of Sn-3.5Ag/Cu solder joint with high fraction of intermetallic compounds: experimental analysis. *J. Alloys Compd.* 680, 665–676 (2016).
7. H.T. Lee, M.H. Chen, H.M. Jao, and T.L. Liao, Influence of interfacial intermetallic compound on fracture behavior of solders joints. *Mater. Sci. Eng. A.* 358, 134–141 (2003).
8. H. Zou, Q. Zhu, and Z. Zhang, Growth kinetics of intermetallic compounds and tensile properties of Sn-Ag-Cu/Ag single crystal joint. *J. Alloy. Compound.* 461, 410–417 (2008).
9. K.S. Kim, S.H. Huh, and K. Suganuma, Effects of cooling speed on microstructure and tensile properties of Sn-Ag-Cu alloys. *Mater. Sci. Eng. A.* 333, 106–114 (2002).
10. F. Ochoa, J.J. Williams, and N. Chawla, Effects of cooling rate on the microstructure and tensile behavior of a Sn-3.5wt.%Ag solder. *J. Electron. Mater.* 32, 1414–1420 (2003).
11. J. Shen, Y.C. Liu, H.X. Gao, C. Wei, and Y.Q. Yang, Formation of bulk Ag_3Sn intermetallic compounds in SnAg lead-free solders in solidification. *J. Electron. Mater.* 34, 1591–1597 (2005).
12. J.H. Lee, A.M. Yu, J.H. Kim, M.S. Kim, and N. Kang, Reaction properties and interfacial intermetallics for $Sn_xAg_{0.5}Cu$ solders as a function of Ag content. *Met. Mater. Int.* 14, 649–654 (2008).
13. Z. Zhu, H. Sun, F. Wu, and Y.-C. Chan, Comparative study of the microstructure and mechanical strength of tin-copper($Sn_{0.7}Cu$) solder modified with silver(Ag) by both alloying and doping methods. *J. Mater. Sci: Mater. Electron.* 27, 6835–6844 (2016).
14. K.J. Rnk, F. Loo, and J.K. Kivilahti, A diffusion-kinetic model for predicting solder/conductor interactions in high density interconnections. *Metall. Mater. Trans. A.* 29, 2951–2956 (1998).
15. X. Ma, F. Wang, Y. Qian, and F. Yoshida, Development of Cu-Sn intermetallic compound at Pb-free solder/Cu joint interface. *Mater. Lett.* 57, 3361–3365 (2003).
16. T. Laurila, J. Hurtig, and V. Vuorinen, Effect of Ag, Fe, Au and Ni on the growth kinetics of Sn-Cu intermetallic compound layers. *Microelectron. Reliab.* 49, 242–247 (2009).
17. D.Q. Yu, L. Wang, C.M.L. Wu, and C.M. Law, T The formation of nano-Ag_3Sn particles on the intermetallic compounds during wetting reaction. *J. Alloy. Comp.* 389, 153–158 (2005).